Development of an Analytical Quantum Full-Wave Solution for a Transmon Qubit in a 3D Cavity

Soomin Moon* and Thomas E. Roth*†

*Elmore Family School of Electrical and Computer Engineering, West Lafayette, Indiana 47906, USA †Purdue Quantum Science and Engineering Institute, West Lafayette, Indiana 47907, USA, rothte@purdue.edu

Abstract—Circuit quantum electrodynamics is one of the most promising platforms for building quantum information processors. To meet the stringent performance requirements, high-fidelity general-purpose numerical methods are increasingly needed to improve designs. Currently, there exist a limited number of methods for analyzing these systems and they suffer from problematic efficiency limitations. One challenge in developing more efficient methods is the lack of available reference data that can be generated to validate them. Here, we develop an analytical quantum full-wave solution for a transmon qubit in a 3D cavity that can validate numerical methods in the future. We start by reviewing the basics of the field-based quantization method used before showing how classical electromagnetic theories can be used to analytically evaluate all field-based parameters in our formulation. We validate our analytical solution by calculating experimentally-relevant system parameters and comparing against approaches that use numerical EM eigenmodes in their solution.

Index Terms—Circuit quantum electrodynamics, transmon qubit, quantum theory, microwave resonators, cavity perturbation theory, and antenna theory.

I. INTRODUCTION

Quantum information processing devices have the potential to revolutionize computing due to their unmatched performance compared to classical computers on important classes of difficult computational tasks. The circuit quantum electrodynamics (cQED) platform using transmon quantum bits (qubits) [1], [2] is one of the most promising architectures for building quantum information processors, whose maturity was recently demonstrated through landmark achievements of a quantum advantage compared to classical technologies [3], [4]. However, substantial improvements are still needed for these technologies to address practical problems of interest, which requires component-level design improvements while massively scaling the number of qubits in the system [5], [6]. To overcome these engineering challenges, general-purpose and high-fidelity numerical analysis tools are becoming increasingly important for optimizing designs [7].

Currently, one of the few general-purpose numerical methods available is the energy participation ratio (EPR) quantization method [7]. In this approach, all quantities in the quantum Hamiltonian describing a system are related to results of a linear electromagnetic (EM) eigenmode analysis of the geometry being considered. Although the EPR method has been validated for systems involving multiple transmon qubits [1], [2], the computational cost of the EM eigenmode analysis

is problematic for analyzing large-scale systems. Further, as will be shown later, the method requires the use of a large quantum state space to reach numerical convergence that also significantly limits the size of system that can be analyzed in practice.

An alternative method to EPR quantization is the field-based quantization approach for cQED systems proposed in [8]. In this formalism, key parameters in the quantum Hamiltonian describing a system can also be evaluated in terms of results of a linear EM eigenmode analysis. However, due to differences in how qubits are incorporated into this formalism, a much smaller quantum state space can be used to reach numerical convergence for an accurate solution, as will be shown later.

Both aforementioned methods rely on numerically finding EM eigenmodes, which becomes computationally prohibitive for large devices. As a result, there is a need for more efficient methods to be formulated. Since measured data is not a widely-available resource and numerically performing a 3D EM eigenmode analysis can also be prohibitive, it becomes difficult to validate new numerical methods as they are developed. To help address this, we have designed a simple geometry for which all field-based aspects of the quantum Hamiltonian proposed in [8] can be evaluated analytically using results from cavity perturbation theory [9] and antenna theory [10]. In the future, this analytical solution can be used to validate new numerical methods, as well as build intuition about important quantum effects that occur in cQED devices.

The remainder of this work is organized in the following manner. In Section II, we review the necessary basics of the field-based quantization approach used in this work. Following this, in Section III we introduce the system geometry and then discuss how traditional analytical EM theories can be used to evaluate the parameters in the total system Hamiltonian. Next, we present numerical results in Section IV to validate our analytical solution against an implementation of our theory using numerical EM eigenmodes and the EPR method. Finally, we discuss conclusions and future work in Section V.

II. BACKGROUND

Before discussing the formulation of our analytical solution, it is necessary to review some basics of the field-based quantization method discussed in [8]. There, the quantum

Hamiltonian for a general system composed of a transmon qubit [1], [2] coupled to the quantum EM field is given as

$$\hat{H} = \hat{H}_F + \hat{H}_T + \hat{H}_I,\tag{1}$$

where \hat{H}_F corresponds to the total energy of the EM field, \hat{H}_T is transmon energy, and \hat{H}_I is the interaction Hamiltonian describing the coupling between the two subsystems. For an introduction to Hamiltonian methods in electromagnetics, see [11] and references therein. Also, note that "hats" in this work denote quantum operators rather than geometric unit vectors.

More specifically, the EM field Hamiltonian is

$$\hat{H}_F = \frac{1}{2} \iiint \left(\epsilon \hat{\mathbf{E}}^2 + \mu \hat{\mathbf{H}}^2 \right) d\mathbf{r},\tag{2}$$

where $\hat{\mathbf{E}}$ and $\hat{\mathbf{H}}$ are quantum electric and magnetic field operators. These operators can be expressed in many different ways, but here we will consider them in terms of eigenmodes found by solving the EM wave equation as an eigenvalue problem. In this case, the field operators are

$$\hat{\mathbf{E}}(\mathbf{r}) = \sum_{k} \sqrt{\frac{\hbar \omega_k}{2\epsilon_0}} (\hat{a}_k + \hat{a}_k^{\dagger}) \mathbf{E}_k(\mathbf{r}), \tag{3}$$

$$\hat{\mathbf{H}}(\mathbf{r}) = -i \sum_{k} \sqrt{\frac{\hbar \omega_k}{2\mu_0}} (\hat{a}_k - \hat{a}_k^{\dagger}) \mathbf{H}_k(\mathbf{r}), \tag{4}$$

where ω_k is an eigenfrequency, \mathbf{E}_k and \mathbf{H}_k are orthonormal field modes, and \hat{a}_k^{\dagger} and \hat{a}_k are the creation and annihilation operators of the kth field mode [8].

Next, the transmon Hamiltonian is

$$\hat{H}_T = 4E_C \hat{n}^2 - E_J \cos \hat{\varphi},\tag{5}$$

which from a circuit theory perspective corresponds to a linear capacitor in parallel with a nonlinear inductor. Here, \hat{n} and $\hat{\varphi}$ are the qubit charge and phase operators that serve as canonically conjugate operators for the qubit [1], [2]. Further, $E_C=e^2/(2C_\Sigma)$ is the charging energy of the total qubit capacitance C_Σ , where e is the electron charge. We also have that the Josephson energy is $E_J=(\hbar/2e)^2/L_J$, where L_J is the Josephson inductance. For a transmon, the energy parameters are designed such that $E_J/E_C\gg 1$ to minimize the qubit sensitivty to a common form of noise [1], [2].

Finally, the interaction Hamiltonian is

$$\hat{H}_I = 2e \iiint \hat{\mathbf{E}} \cdot \mathbf{d}(\mathbf{r}) \hat{n} d\mathbf{r}, \tag{6}$$

where \mathbf{d} parameterizes a line integration path so that its integral with $\hat{\mathbf{E}}$ computes the voltage seen by the Josephson junction in the transmon qubit [8].

At this point, it is useful to simplify (1) by substituting in (3) and (4) and evaluating the spatial integrals leveraging the orthonormality of the field modes. Further, it is convenient to re-express the transmon operators in terms of the qubit states that are eigenstates of the transmon Hamiltonian given in (5). Denoting the jth eigenstate in Dirac bra-ket notation as $|j\rangle$ and

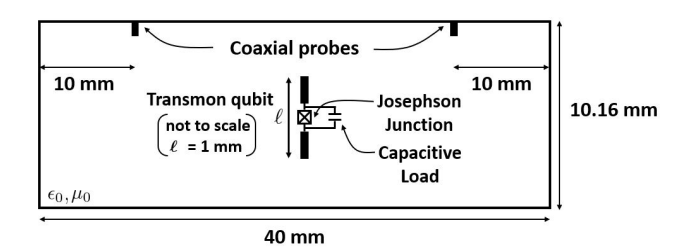


Fig. 1. Schematic illustration of a transmon qubit embedded in a rectangular waveguide cavity structure that is analytically solvable for all field-based aspects of the quantum full-wave Hamiltonian analysis.

its "Hermitian conjugate" as $\langle j|$, we can eventually simplify (1) to

$$\hat{H} = \sum_{k} \hbar \omega_{k} \hat{a}_{k}^{\dagger} \hat{a}_{k} + \sum_{j} \hbar \omega_{j} |j\rangle\langle j|$$

$$+ \sum_{k,j} \left(\hbar g_{k,j} \hat{a}_{k}^{\dagger} |j\rangle\langle j+1| + \hbar g_{k,j}^{*} \hat{a}_{k}^{\dagger} |j+1\rangle\langle j| \right), \quad (7)$$

where we have also applied the "rotating wave approximation" to drop terms that are unimportant in the operating regime considered in Section IV and noted that the charge operator approximately only allows transitions between nearest-neighbor energy eigenstates for transmon qubits [1]. Further, ω_j is the qubit eigenfrequency associated with energy eigenstate $|j\rangle$ and $g_{k,j}$ is the coupling rate between specific field and transmon modes given by

$$g_{k,j} = 2e\langle j|\hat{n}|j+1\rangle\sqrt{\frac{\omega_k}{2\epsilon_0\hbar}} \iiint \mathbf{E}_k(\mathbf{r}) \cdot \mathbf{d}(\mathbf{r})d\mathbf{r}.$$
 (8)

In the next section, we will show how all of the EM field-dependent parameters discussed throughout this section can be evaluated using analytical methods of classical EM theory for an appropriately-designed system geometry.

III. FORMULATION

So the parameters of the total Hamiltonian can be evaluated in an analytical manner, we have considered the simple geometry shown in Fig. 1. This system is inspired by cQED structures that have been experimentally studied in the past that are often referred to as 3D transmons [12], which consist of a transmon qubit formed by a small planar dipole antenna that is embedded in a waveguide cavity. For our system, we have made the cavity a rectangular waveguide due to the simplicity of the field distributions [9] and formed the transmon from a small wire dipole antenna so typical antenna theory techniques can be leveraged in our analytical solution [10]. Further, we developed our geometry in the broader context of the modematching (or projector-based) quantization approach of [8] that is useful for analyzing systems with ports, so we have included two coaxial probes in our geometry that would facilitate coupling to ports as in [13]. These ports would typically be used to control the system with microwave drives; however, this will not be considered directly here.

As alluded to previously, the transmon in our system is composed of a linear wire dipole antenna that has a Josephson junction and an additional load capacitance connected in parallel across the dipole's terminals. The Josephson junction itself can be considered to be composed of a linear junction capacitance and a nonlinear inductance. In our system, we keep the length of the dipole electrically small compared to the variation of the relevant cavity field modes. This then makes the cavity field modes appear effectively like plane waves to the dipole antenna so that typical antenna theory formulas developed for free space operation can still be applied for the dipole in the cavity, as will be substantiated by the numerical results in Section IV.

We will now summarize how the different parameters in the total system Hamiltonian of (7) can be evaluated using traditional EM theories. To begin, we will consider computing the cavity resonant frequency ω_k . Based on the field quantization process [8], we need to determine ω_k in the absence of the transmon, which leaves only the perturbation due to the coaxial probes to be accounted for. Due to the small size of the coaxial probes, their effect on ω_k can be determined using cavity perturbation theory for "shape perturbations" [9]. In this case, the resonant frequency of the cavity including the effect of perturbation is evaluated as

$$\omega_k \approx \omega_k' + \omega_k' \frac{\int_{\Delta V} (\mu |\mathbf{H}_k|^2 - \epsilon |\mathbf{E}_k|^2) dV}{\int_{V} (\mu |\mathbf{H}_k|^2 + \epsilon |\mathbf{E}_k|^2) dV}, \tag{9}$$

where ω_k is the perturbed resonant frequency, ω_k' is the unperturbed resonant frequency (i.e., of the empty cavity), V is the volume of the unperturbed cavity, ΔV is the volume of the perturbation corresponding to the coaxial probes, \mathbf{E}_k and \mathbf{H}_k are the EM fields of the unperturbed cavity for the kth field mode, and μ and ϵ are the constitutive parameters of the material inside the cavity (free space in the case considered here). We integrated the EM energy over the coaxial probes by sampling the EM field at the tips of the coaxial probes and multiplying by the volume of the probe [9], which is reasonable for the lower cavity modes considered in our solution that do not vary along the length of the coaxial probes.

Next, the eigenfrequencies of the transmon ω_j in (7) will be considered. In typical scenarios, E_J is a given parameter that depends on the microscopic structure of the Josephson junction and is not influenced by the surrounding geometry. Hence, the only other parameter needed to characterize the transmon is E_C , which is a function of the total capacitance in parallel to the Josephson junction. Here, this is

$$C_{\Sigma} = C_{\text{ant}} + C_J + C_{\ell} \tag{10}$$

where $C_{\rm ant}$ is the geometric capacitance of the dipole antenna, C_J is the linear Josephson junction capacitance, and C_ℓ is the load capacitance due to a lumped element placed across the dipole terminals. This load capacitance is needed to boost the total qubit capacitance so that the qubit operates in the "transmon regime" where $E_J/E_C\gg 1$. Since C_J and C_ℓ

are given parameters in a design, the only capacitance that actually needs to be determined from the geometry of the system is $C_{\rm ant}$. For a small dipole antenna, this capacitance can be computed using

$$C_{\text{ant}} = \frac{\tan(kL/2)}{120\omega_k(\ln(L/(2r)) - 1)},$$
 (11)

where L is the length of the dipole, r is the radius of the cylinder of the dipole, k is the free space wave number, and ω_k is the operating frequency of the fundamental mode of the cavity [10]. With E_C and E_J determined, they can be used to calculate the eigenfrequencies of the transmon either analytically [1] or numerically. In our work, we have used a simple finite element method to compute the eigenfrequencies of the transmon as described in [14].

Lastly, evaluating the coupling rate $g_{k,r}$ in (8) can be started by evaluating the transition matrix element of the charge operator, $\langle j|\hat{n}|j+1\rangle$. This can be computed numerically, or can be approximated analytically as [1]

$$\langle j|\hat{n}|j+1\rangle \approx -i \bigg(\frac{E_J}{8E_C}\bigg)^{1/4} \sqrt{\frac{j+1}{2}}. \eqno(12)$$

The spatial integral in (8) also must be evaluated, and corresponds to computing the voltage induced across the dipole terminals in the absence of the nonlinear inductance of the Josephson junction. To begin, we first use the vector effective length from antenna theory to find the open circuit voltage that would be induced. For a small linear dipole antenna, the open circuit voltage assuming broadside incidence is

$$V_{\rm oc} = \frac{1}{2} \,\tilde{\ell} \cdot \mathbf{E}_k(\mathbf{r}_0) L \tag{13}$$

where $\tilde{\ell}$ is a unit vector pointing along the length of the dipole and \mathbf{r}_0 is the position at the center of the dipole [10]. Then, the voltage induced across the dipole terminals accounting for the load capacitances can be found by performing a voltage division as

$$V_{\rm t} = V_{\rm oc} \frac{C_{\rm ant}}{C_{\rm ant} + C_{\ell}}.$$
 (14)

With all the parameters in the Hamiltonian operator now determined, a matrix representation of it can be found in terms of a suitable basis [15]. Here, we will form our basis as a tensor product between the "natural" basis of each of the constituent parts of the system. For the qubit, this corresponds to its free energy levels, denoted by $|j\rangle$ for j an integer in the range [0,J-1]. Similarly, each cavity mode is expressed in terms of its own eigenstates that correspond to a fixed number of photons in the mode (these are typically referred to as *Fock states*). The matrix representation of \hat{H} is then found by evaluating

$$H_{mn} = \langle m|\hat{H}|n\rangle,\tag{15}$$

where H_{mn} is the element in the mth row and nth column of the matrix and $|m\rangle$ and $|n\rangle$ are two states of the tensor product basis being used. In any calculation, it is imperative that a sufficiently large basis is used to achieve numerically converged results for the system parameters of interest.

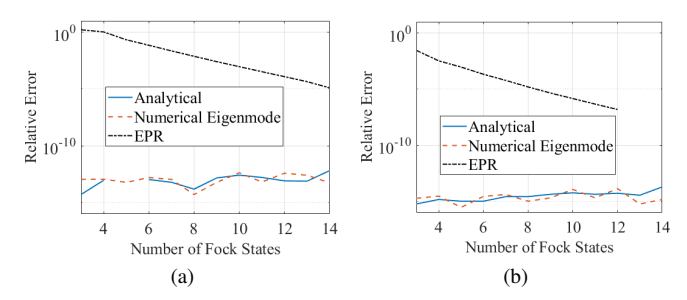


Fig. 2. Numerical convergence of the different computation methodologies for (a) the qubit anharmonicity α and (b) the first qubit transition frequency ω_{01} . The reference solution for each computation method is its own results using 15 Fock states for each mode in the basis.

IV. NUMERICAL RESULTS

Our simulation is considered for a geometry as shown in Fig. 1 . The dimensions of the cavity are $22.86 \times 10.16 \times$ 40 mm³, and the cavity is filled with vacuum. The coaxial probes have a radii of 0.05 mm and lengths of 0.75 mm. The transmon consists of a linear dipole antenna with length 1 mm, radius 0.04 mm, and terminal gap size 0.102 mm that is oriented along the electric field direction of the dominant cavity modes. Also, a load capacitance of 50 fF is included across the dipole terminals. The Josephson junction of the transmon has properties of $L_J=9.40\,\mathrm{nH}$ and $C_J=0.34\,\mathrm{fF}$. For our simulations we will only consider the lowest two cavity modes, which for this system are the TE_{101} and TE_{102} modes. Further, in our analysis, we move the transmon over one quadrant of the cross-sectional plane held at a fixed vertical position of the cavity with each transmon location corresponding to an independent solution.

These system parameters have been selected so that our device operates in the *dispersive regime* of cQED, which is the common operating regime of most practical devices. This regime is characterized by having the detuning between cavity resonant frequencies and qubit transition frequencies being large relative to their coupling; i.e., $\Delta_{k,j} = |\omega_k - \omega_{j,j+1}| \gg |g_{k,j}|$, where $\omega_{j,j+1} = \omega_{j+1} - \omega_j$ is the qubit transition frequency between states $|j\rangle$ and $|j+1\rangle$. In this regime, strong quantum interactions between the cavity and qubit are suppressed, which has certain advantages for controlling and measuring the state of the qubit [16].

To test our solution approach, we have computed various system parameters of experimental relevance for a cQED system operated in the dispersive regime. In particular, we compute the first qubit transition frequency ω_{01} , the qubit anharmonicity $\alpha=\omega_{12}-\omega_{01}$, the cavity resonant frequencies ω_1 and ω_2 , and the AC-Stark shift χ [16]. This final parameter characterizes the interaction strength between the qubit and cavity modes in the dispersive regime, and is important for designing qubit state measurement protocols.

As an initial test, we consider the numerical convergence of typical system parameters as a function of the number of basis states used for the qubit and cavity modes. These convergence plots are shown in Fig. 2 for α and ω_{01} computed using three

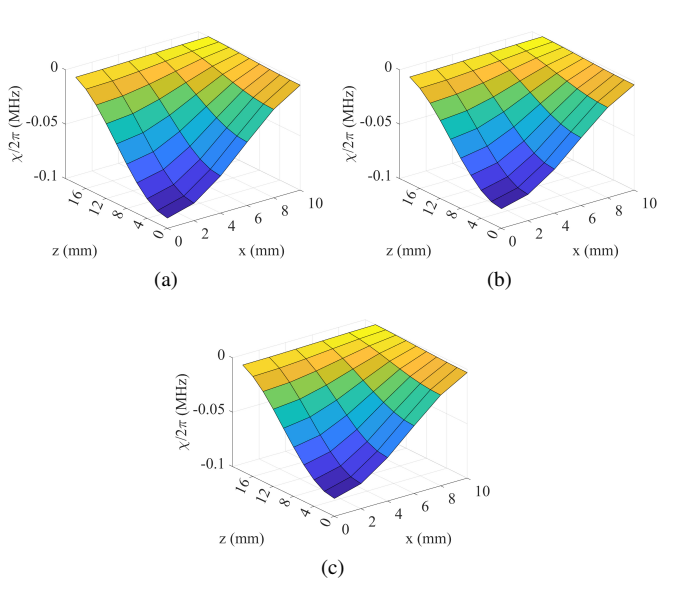


Fig. 3. AC-Stark shift χ computed while moving the transmon over one quadrant of the cross-sectional plane at a fixed vertical position in the cavity center for (a) analytical, (b) numerical eigenmode, and (c) EPR solution methods

different methods. In particular, for our analytical solution, an implementation of our field-based Hamiltonian where all parameters are computed using numerical EM eigenmodes of the cavity, and the EPR method. The relative error is computed for each method by comparing to the results of its own calculation using 15 Fock states for each mode in the basis. From the results, it is clear that the field-based approach described here converges immediately with the lowest number of possible Fock states while the EPR method requires a substantial number of Fock states to converge. We attribute our formulation's quick convergence to explicitly incorporating the nonlinearity of the qubit in the analysis of the qubit subsystem in formulating our Hamiltonian matrix. In constrast, the EPR method treats the nonlinear effects as a perturbation to the linear effects, which then requires a large number of Fock states to be considered to achieve convergence even in the properties of the lowest energy levels of the system. Since the size of the Hamiltonian matrix grows exponentially with the number of Fock states considered, achieving fast numerical convergence is a key property for a numerical method. For the remaining results, we use 8 Fock states for all methods to compare results fairly.

Next, we show the effect of moving the transmon throughout the cavity on χ , which is sensitive to these movements. This is shown in Fig. 3, where it is clear that all methods demonstrate similar behavior due to the coupling to the dominant ${\rm TE}_{101}$ mode. This also highlights that the approximations in the analytical solution do not break down so long as the dipole is kept a few millimeters away from the walls of the cavity.

Finally, we summarize the relative error of all computed dispersive regime parameters in Table I. Here, the dispersive regime parameters are averaged as a function of the transmon

TABLE I
AVERAGE SYSTEM PARAMETERS AND RELATIVE PERCENT ERRORS WITH
RESPECT TO THE NUMERICAL EIGENMODE DATA

System Parameter	Numerical Eigenmode	EPR	Analytical Solution
$\omega_{01}/2\pi$ (GHz)	6.44	6.43 (0.21)	6.39 (0.84)
$\omega_1/2\pi$ (GHz)	7.55	7.55 (8.82e-5)	7.55 (1.5e-2)
$\omega_2/2\pi$ (GHz)	9.96	9.96 (8.88e-5)	9.96 (2.6e-2)
$\alpha/2\pi$ (MHz)	-379.00	-360.78 (-4.81)	-371.72 (-1.92)
$\chi/2\pi$ (MHz)	-0.025	-0.026 (-2.23)	-0.028 (-10.38)

location in the cavity. Relative errors are also computed between the methods as compared to the numerical eigenmode solution of our field-based formulation, which are shown in parentheses in Table I. Given the typical experimental precision, the relative errors are within reasonable ranges [7]. The main source of error in our analytical solution has been found to be due to the approximation of the capacitance of the dipole antenna from (11). With a better estimation of this capacitance, the accuracy of the analytical solution can become much closer to that of the numerical eigenmode approach for this geometry.

V. CONCLUSION

This work presented an analytical quantum full-wave solution for a transmon qubit in a rectangular waveguide cavity using a field-based quantization approach. The analytical solution utilized the classical EM methods of cavity perturbation theory and antenna theory to evaluate all the field-based aspects of the Hamiltonian of the system. This approach was shown to be valid by computing experimentally-relevant system parameters and comparing them to an implementation of the same theory using numerical EM eigenmodes and to the independent EPR quantization method. Future work can involve extending the analytical quantum full-wave solution to include multiple qubits, improving its accuracy using more sophisticated classical EM theories, and applying similar techniques to more complicated geometries.

ACKNOWLEDGEMENT

This material is based upon work supported by the National Science Foundation under Grant No. 2202389 and Purdue ECE Elmore Emerging Frontiers Center "The Crossroads of Quantum and AI."

REFERENCES

- [1] J. Koch, M. Y. Terri, J. Gambetta, A. A. Houck, D. Schuster, J. Majer, A. Blais, M. H. Devoret, S. M. Girvin, and R. J. Schoelkopf, "Chargeinsensitive qubit design derived from the Cooper pair box," *Physical Review A*, vol. 76, no. 4, p. 042319, 2007.
- [2] T. E. Roth, R. Ma, and W. C. Chew, "The transmon qubit for electromagnetics engineers: An introduction," *IEEE Antennas and Propagation Magazine*, 2022.
- [3] F. Arute, K. Arya, R. Babbush, D. Bacon, J. C. Bardin, R. Barends, R. Biswas, S. Boixo, F. G. Brandao, D. A. Buell *et al.*, "Quantum supremacy using a programmable superconducting processor," *Nature*, vol. 574, no. 7779, pp. 505–510, 2019.

- [4] Y. Wu, W.-S. Bao, S. Cao, F. Chen, M.-C. Chen, X. Chen, T.-H. Chung, H. Deng, Y. Du, D. Fan et al., "Strong quantum computational advantage using a superconducting quantum processor," *Physical Review Letters*, vol. 127, no. 18, p. 180501, 2021.
- [5] P. Jurcevic, A. Javadi-Abhari, L. S. Bishop, I. Lauer, D. F. Bogorin, M. Brink, L. Capelluto, O. Günlük, T. Itoko, N. Kanazawa et al., "Demonstration of quantum volume 64 on a superconducting quantum computing system," *Quantum Science and Technology*, vol. 6, no. 2, p. 025020, 2021.
- [6] R. Acharya, I. Aleiner, R. Allen, T. I. Andersen, M. Ansmann, F. Arute, K. Arya, A. Asfaw, J. Atalaya, R. Babbush *et al.*, "Suppressing quantum errors by scaling a surface code logical qubit," *Nature*, vol. 614, no. 7949, pp. 676–681, Feb 2023.
- [7] Z. K. Minev, Z. Leghtas, S. O. Mundhada, L. Christakis, I. M. Pop, and M. H. Devoret, "Energy-participation quantization of Josephson circuits," npj Quantum Information, vol. 7, no. 1, pp. 1–11, 2021.
- [8] T. E. Roth and W. C. Chew, "Macroscopic circuit quantum electrodynamics: A new look toward developing full-wave numerical models," *IEEE Journal on Multiscale and Multiphysics Computational Techniques*, vol. 6, pp. 109–124, 2021.
- [9] D. M. Pozar, Microwave Engineering. John Wiley & Sons, 2009.
- [10] C. A. Balanis, Antenna Theory: Analysis and Design. John Wiley & Sons, 2016.
- [11] W. C. Chew, D. Y. Na, P. Bermel, T. E. Roth, C. J. Ryu, and E. Kudeki, "Quantum Maxwell's equations made simple: Employing scalar and vector potential formulation," *IEEE Antennas and Propagation Magazine*, vol. 63, no. 1, pp. 14–26, 2021.
- [12] H. Paik, D. I. Schuster, L. S. Bishop, G. Kirchmair, G. Catelani, A. P. Sears, B. Johnson, M. Reagor, L. Frunzio, L. I. Glazman et al., "Observation of high coherence in Josephson junction qubits measured in a three-dimensional circuit QED architecture," *Physical Review Letters*, vol. 107, no. 24, p. 240501, 2011.
- [13] S. Moon and T. E. Roth, "Validation of the full-wave projector-based Hamiltonian analysis of port-driven microwave resonators," in 2023 Photonics & Electromagnetics Research Symposium (PIERS). IEEE, 2023, pp. 1180–1188.
- [14] T. E. Roth, "Finite element time domain discretization of a semiclassical Maxwell-Schrödinger model of a transmon qubit," in 2023 IEEE MTT-S International Conference on Numerical Electromagnetic and Multiphysics Modeling and Optimization (NEMO). IEEE, 2023, pp. 95–98.
- [15] D. A. B. Miller, Quantum Mechanics for Scientists and Engineers. Cambridge University Press, 2008.
- [16] P. Krantz, M. Kjaergaard, F. Yan, T. P. Orlando, S. Gustavsson, and W. D. Oliver, "A quantum engineer's guide to superconducting qubits," *Applied Physics Reviews*, vol. 6, no. 2, p. 021318, 2019.